### Title

Whither Mn Oxidation in Mn-Rich Alkali-Excess Cathodes?




### Journal

ACS Energy Letters, 6(3)

### ISSN

2380-8195



### Authors

Zuba, Mateusz Jan
Grenier, Antonin
Lebens-Higgins, Zachary
et al.



### Publication Date

2021-03-12

### DOI

10.1021/acsenergylett.0c02418

Peer reviewed

# Whither Mn Oxidation in Mn-Rich Alkali-Excess Cathodes?

Mateusz Jan Zuba, Antonin Grenier, Zachary Lebens-Higgins, Galo J. Paez Fajardo, Yixuan Li, Yang Ha, Hui Zhou, M. Stanley Whittingham, Wanli Yang, Ying Shirley Meng, Karena W. Chapman, and Louis F. J. Piper*

**ABSTRACT:** **Lithium-rich NMC (LR-NMC) compounds exhibit high capacities beyond the traditional redox, but it remains unclear whether the anomalous charge compensation mechanism is due to oxidized lattice oxygen or migration-assisted Mn oxidation. We compare LR-NMC with a model $Mn^{7+}$ system ($KMnO_4$) using a combination of resonant inelastic X-ray scattering (RIXS) irradiation studies and *operando* X-ray absorption spectroscopy/X-ray diffraction (XAS/XRD) to quantify transition metal (TM) migration, Mn oxidization, and beam-induced effects. We reveal how for $KMnO_4$ it is possible to observe beam-induced Mn reduction resulting in trapped molecular oxygen. For LR-NMC, we observe negligible evidence for Mn oxidation while stabilized tetrahedral sites correlate more with a reduced TM environment. Finally, the additional spectroscopic structures observed in oxidized oxygen RIXS for LR-NMC are absent for gas-phase molecular oxygen.**

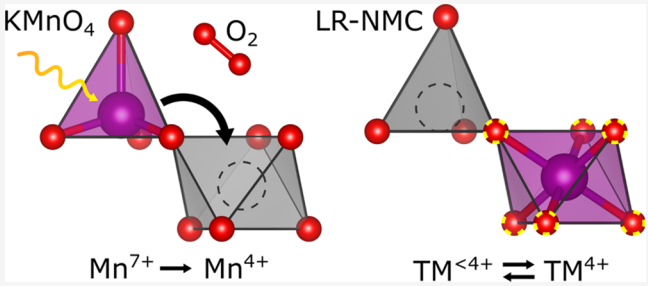


High energy densities of lithium-ion batteries have enabled several highly utilized comercial applications.[1] Extensive efforts are being made to increase energy density of cathode materials by moving away from typical $LiMO_2$ (M = Ni, Co, Mn, Al) systems toward lithium-rich, $xLi_2MnO_3*(1-x)LiMO_2$ (M= Mn, Ni, Co).[2−5] Initially considered to be anionic redox active because of the $Li_2MnO_3$ component, these Li-rich materials are plagued with severe voltage hystersis and fade issues on the first and subsequent cycles.[6] The cause of this voltage fade in lithium-rich systems has been shown experimentally,[7,8] and from first-principles thermodynamics,[9] to be largely attributed to transition metal (TM) migration, and more recently Li migration,[10] from the TM layer into empty Li sites. However, the underlying charge compensation mechanism behind their anomalous capacity remains hotly debated, which can be categorized into oxidized oxygen, exotic Mn oxidation, gas evolution, or some combination of the above. In this Letter, we use the term lattice oxygen redox to refer to O-holes, molecular oxygen to refer to trapped $O_2$ formation, oxygen loss to refer to $O_2$ leaving the lattice, and transition metal migration to refer to out-of-plane migration from the transition metal layer to the lithium layer.

For Li-rich systems, several oxygen sensitive probes (Raman,[11,12] hard X-ray photoelectron spectroscopy (HAXPES),[4] and resonant inelastic X-ray scattering (RIXS)[13−16]) have been employed to detect signatures of oxidized oxygen (either in the form of a peroxo-like O−O dimer or $O^{n-}$ anion). Of these, RIXS is considered the most reliable for tracking bulk oxygen participation with anomalous capacity.[17,18] A recent O K-edge RIXS study by House *et al.* has suggested trapped molecular oxygen redox as a candidate.[19] Radin *et al.* proposed Mn oxidation from 4+ to 7+, facilitated by octahedral to tetrahedral migration, as an explanation for the anomalous charge compensation in $Li_2MnO_3$,[20] and by extension Li-rich compounds containing $Li_2MnO_3$ as a nanocomposite. Such a highly oxidized environment could decompose, resulting in Mn reduction and the subsequent formation of molecular oxygen. Recent differential electrochemical mass spectrometry (DEMS) quantitative studies have shown that the charge compensation behind $Li_2MnO_3$ is largely due to oxygen loss from the cathode surface,[21,22] while at the same time it lacked an oxidized oxygen feature in the corresponding RIXS measurements.[21−23] In contrast to $Li_2MnO_3$, LR-NMC exhibits significantly less

oxygen loss and only at high potentials,[13,24−26] which suggests a different charge compensation mechanism is occurring. Although there is no experimental report of Mn oxidation in $Li_2MnO_3$,[21] a migratory $Mn^{7+}$ could potentially be stabilized in LR-NMC or serve as a reaction intermediate for the formation of trapped molecular oxygen.[20] While not limited to $Mn^{4+/7+}$ redox mechanism, transition metal migration has been proposed by Gent *et al.* and Bruce *et al.* as necessary for facilitating oxidized oxygen in Li-rich systems.[8,14,27] It remains unclear whether transition metal migration is responsible for oxidized oxygen RIXS features by either facilitating oxidized oxygen or indirectly through decomposition (*i.e.*, formation of trapped molecular oxygen).

In this study, we quantify the extent of transition metal migration, Mn oxidation, and beam-induced degradation in LR-NMC to determine whether transition metal migration is facilitating O K-edge RIXS features. By using a model $Mn^{7+}$ compound ($KMnO_4$), we observe an irreversible X-ray-induced degradation pathway from tetrahedral $Mn^{7+}$ to trapped molecular oxygen in high energy transfer rate soft X-ray studies. For LR-NMC, we employed higher-energy X-ray techniques with lower-energy transfer rate (*operando* XANES and XRD) to circumvent beam-induced effects and determine upper limits of oxidation above $Mn^{4+}$ and the extent of transition metal migration to tetrahedral/octahedral sites to the Li layer. No evidence of significant Mn oxidation was observed in our *operando* Mn K-edge XANES. The transition metal migration in LR-NMC comparable to that of classical layered oxide NMC 442 from our XRD measurements suggests other mechanisms beyond Mn oxidation can give rise to migration into the tetrahedral sites. As a result, our data rules against beam-induced $Mn^{7+}$ to trapped molecular oxygen for LR-NMC. Furthermore, the RIXS response to X-ray beam exposure for LR-NMC is different from that observed in $KMnO_4$, while also displaying additional features that are absent for molecular oxygen. We conclude that the intrinsic O K-edge RIXS features of LR-NMC[28] are not associated with molecular oxygen species originating from beam-induced reduction of $Mn^{7+}$.

High-quality Li-rich NMC ($Li[Li_{0.144}Ni_{0.136}Mn_{0.544}Co_{0.136}]O_2$) was synthesized by the coprecipitation method. A detailed synthesis procedure can be found in a previous publication.[29] Commercial NMC 442 ($LiNi_{0.40}Mn_{0.40}Co_{0.20}O_2$) and NMC 811 ($LiNi_{0.80}Mn_{0.10}Co_{0.10}O_2$) were obtained from Toda America and Ecopro Co., Ltd., respectively. Commercial $KMnO_4$ was purchased from Sigma-Aldrich. Details regarding principal component analysis (PCA) of $KMnO_4$ RIXS, materials preparation, experimental methods, as well as structural models used for XRD analysis in this study can be found in Supporting Information.

As shown in Figure 1a, representative electrochemistry of an LR-NMC system displays two voltage regimes in the first charge. The initial capacity contributions have been established to be associated with tradition transition metal oxidation ($TM^{2+/3+} \rightarrow TM^{4+}$),[13,30] but the charge compensation in the high-voltage regime (indicated by dashed vertical lines) is the main focus of this work. Oxygen K-edge RIXS has been prominently used to study this high-voltage regime because of the emergence of a loss feature emerging in a variety of delithiated Li-rich systems.[8,14,15,26] Figure 1b shows representative O K-edge RIXS maps of LR-NMC before and after the high-voltage plateau displaying the emergence of a loss feature at an excitation energy of ~531 eV and corresponding

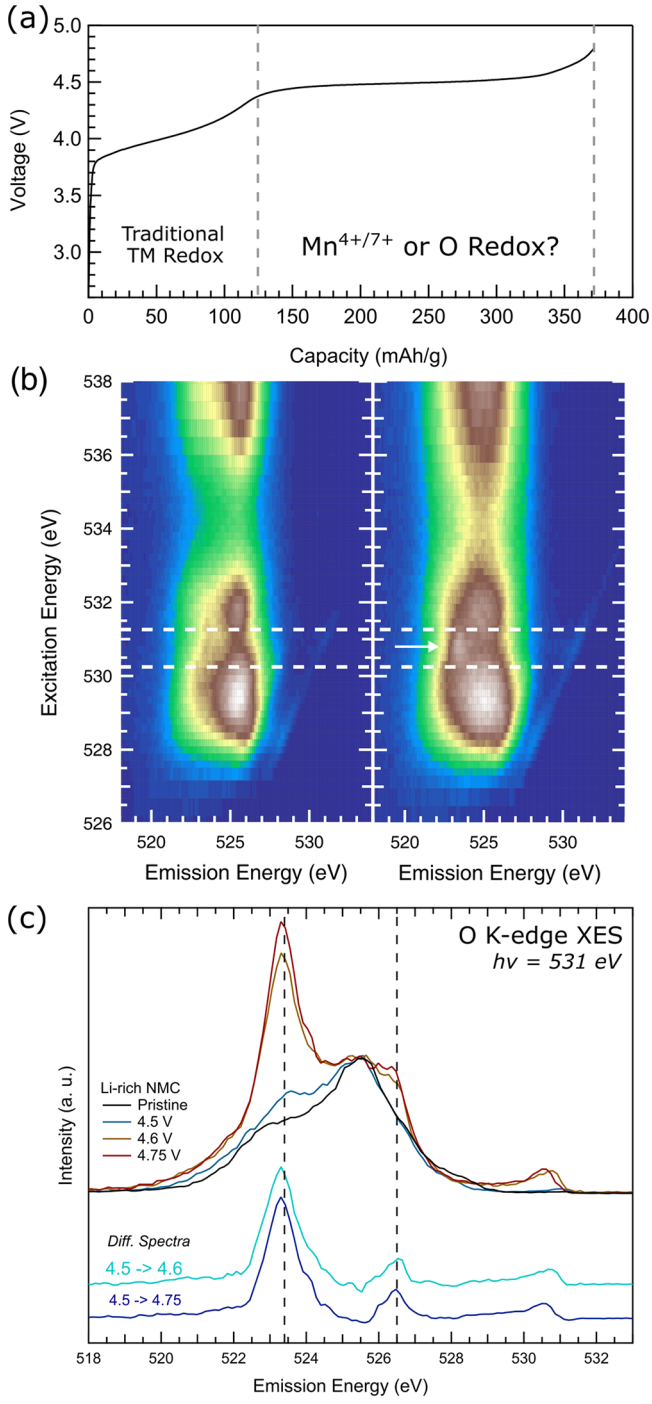


**Figure 1. (a) First charge curve electrochemical profile of LR-NMC depicting two potential regimes. (b) Oxygen K-edge RIXS maps of before (left) and after (right) the high-voltage plateau (>4.4 V) reveal a RIXS feature at an excitation energy of ~531 eV. (c) RIXS emission lines at 531 eV for LR-NMC at different states of charge. Difference spectra between preplateau and points along the plateau are given to highlight changes in the O K-edge RIXS emission line shape. Two vertical lines highlight the two emission features.**

emission energy of ~523.5 eV. While the electronic origin of this RIXS loss feature has been attributed to oxidized lattice oxygen,[18] the true structural origin of this feature has been debated as being between localized electron holes on oxygen,[13,31,32] peroxides,[16] and trapped molecular oxygen.[19]

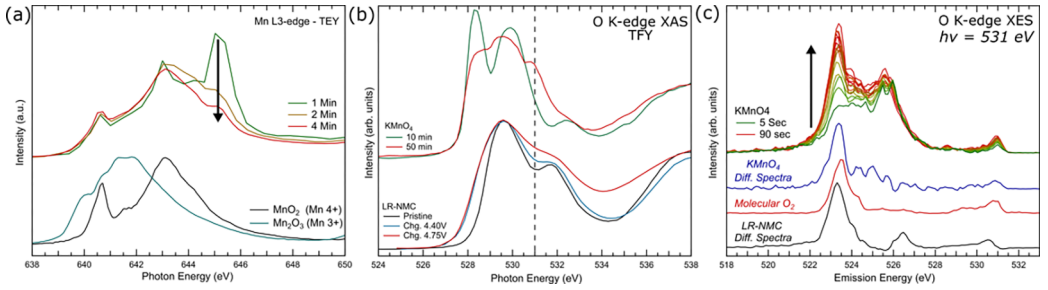


**Figure 2. Time-dependent (a) Mn L3-edge TEY and (b) O K-edges TFY measurements describe the photosensitivity of $KMnO_4$. $MnO_2$, $Mn_2O_3$, and LR-NMC reference spectra are plotted for direct comparison. Successive (c) O K-edge RIXS emission line measurements at 531 eV depict rapid changes in intensity at emission energy of ~523.5 eV. Difference spectra reveal the evolution of oxidized oxygen feature to be photoinduced in $KMnO_4$. Molecular oxygen (reproduced with permission from ref 37, copyright 2020 American Chemical Society) and difference spectra of LR-NMC at ~531 eV are also displayed for comparison. Molecular oxygen and $KMnO_4$ difference spectra lack the second feature at ~526.5 eV, which appears in LR-NMC.**

In addition to the Li-rich systems, RIXS features have been observed in classical Li layered oxides irrespective of Mn content,[33−36] as well as for Na systems.[19] Aside from battery cathode materials, this oxidized oxygen feature also appears in a series of spectroscopic studies of noncathode systems, including molecular oxygen[37,38] and peroxides.[27,32,39]

To shed light on this issue, we take a closer look at the RIXS feature in the form of difference spectra for charged LR-NMC electrodes at excitation energy of 531 eV (Figure 1c). The RIXS emission feature at ~523.5 eV is present in LR-NMC when charged to 4.6 V (midway high-voltage plateau) and continues to grow when charged to 4.75 V (end of high-voltage plateau). Difference spectra show evidence of a second emission feature of lower intensity and higher energy (~526.5 eV). While molecular oxygen has a similar ~523.5 eV,[37,38] it lacks this second feature that is found in LR-NMC as previously noted by Lebens-Higgins *et al.*[17] The two features in the difference spectra more closely resemble the allowed interband transitions predicted for $Li_2O_2$ using first-principles calculations.[39] The intensity ratio between the two RIXS features remains fixed between different charged states, suggesting a single species of oxidized states. The origin of this second feature needs to be accounted for to fully identify the structural nature of the oxidized oxygen environment given its absence in molecular $O_2$. While the oxidized oxygen features are electronically similar to a peroxide, there is limited corresponding structural evidence of a short ~1.5 Å O−O bond.[40]

It has been recently reported that a $Mn^{7+}$ compound ($KMnO_4$) has a ~523.5 eV RIXS feature similar to that of LR-NMC and other cathode systems.[27] While oxidized oxygen RIXS features found in LR-NMC were reported to be intrinsic,[28] we focus on the beam sensitivity of $KMnO_4$. The presence of a feature in $KMnO_4$ opens up the possibility that similar RIXS observations in the literature could be actually $Mn^{4+/7+}$ redox with a favorable Mn decomposition process from 7+ to 4+ followed by the formation of trapped molecular oxygen. Because high-valent Mn systems (>4+) are photosensitive, particularly to synchrotron soft X-rays,[41] we investigated $KMnO_4$ sXAS as a function of beam exposure. In Figure 2a, surface-sensitive Mn L3-edge total electron yield (TEY) measurements verify the photosensitivity of $KMnO_4$ and show significant Mn photoreduction upon X-ray exposure. After several minutes of exposure, the Mn L3 line shape resembles that of a $Mn^{4+}$ system, which can make TEY L-edge measurements unreliable when quantifying $Mn^{7+}$. Meanwhile, bulk sensitive inverse partial fluorescence yield (iPFY) measurements circumvent self-absorption affects in Mn L-edge spectra but require longer exposure times than TEY measurements.

In Figure 2b, the total fluorescence yield (TFY) O K-edge measurements of $KMnO_4$ reveal further evidence of Mn reduction. Pristine $KMnO_4$ has two initial characteristic pre-edge peaks ($e_g$ at ~529 eV and $t_{2g}$ at ~530.5 eV). During the measurements, the $KMnO_4$ experiences Mn photoreduction leading to an overall broadening of the O K-edge spectra and the emergence of an oxidized oxygen feature at ~531 eV. While the initial $KMnO_4$ O K-edge line shape becomes less defined, the low-energy $e_g$ peak still constitutes a large portion of the distorted line shape. This suggests that $KMnO_4$ photoreduction is a continuous process and that significant $KMnO_4$ species and/or a high-valent Mn intermediary remain present even after significant exposure time. Initially the corresponding O K-edge RIXS results display no signatures of RIXS loss feature(s), but even within short data acquisition a beam-induced feature appears. To demonstrate that the oxidized oxygen feature at ~531 eV is not intrinsic to $KMnO_4$, we also performed successive O K-edge RIXS measurements. PCA was employed to increase the signal-to-noise ratio of successive RIXS scans without resorting to increasing measurement time, resulting in Figure 2c. By measuring $KMnO_4$ continuously at the excitation energy of ~531 eV, we photoinduce an oxidized oxygen RIXS feature at emission energy of ~523.5 eV. A subsequent difference spectrum of initial and postexposed $KMnO_4$ reveals the induced feature has a ~523.5 eV emission peak similar to LR-NMC. The lack of a second feature at ~526.5 eV suggests the photoinduced RIXS feature found in $KMnO_4$ resembles molecular oxygen.[38,42] Because of the presence of residual high-valent Mn after X-ray exposure and the high affinity of $MnO_4^{n-}$ groups to react with peroxides, we assign the feature at ~531 eV to be associated with the formation of trapped $O_2$ molecules rather than a peroxide-like or $O^{n-}$ environment. We attribute our understanding of $KMnO_4$ photoreduction in a vacuum setting to that of traditional thermal decomposition of $KMnO_4$:[43]

$$10KMnO_4 \rightarrow 3K_2MnO_4 + K_4Mn_7O_{16} + 6O_2 \quad (1)$$

$$10K_2MnO_4 \rightarrow 6K_3MnO_4 + \frac{1}{2}K_4Mn_8O_{16} + 4O_2 \quad (2)$$

Synchrotron X-ray spectroscopy techniques can deliver high irradiation rates onto materials and can be a concern when performing measurements on highly oxidized systems. Soft XAS/RIXS techniques, in particular RIXS, employ high flux rates coupled with small spot size resulting in high energy transfer rates, which make measurements of high-valent Mn systems challenging. This work takes into account the varying energy transfer rates (*i.e.*, the energy deposited in a volume resulting from the beam spot size and the attenuation length energy deposited as a function of time of time) induced by common X-ray spectroscopy techniques. Table S1 shows that the calculated energy transfer rates for O K-edge measurements done at the ALS is several orders of magnitude higher than those from hard XAS and XRD measurements done at National Synchrotron Light Source (NSLS-II), which is typically mostly due to the shallow penetration depth of soft X-rays.

We therefore circumvented the aforementioned beam-damage effects by employing higher-energy X-ray techniques with lower-energy transfer rates (Table S1). In addition, the hard X-ray XANES and XRD technqiues we employ are bulk sensitive techniques and can be performed *operando*, whereas *operando* soft XAS measurements suffer from UHV requirements and are still in their infancy. For these reasons, we turn toward hard XAS and XRD to quantify $Mn^{7+}$ in LR-NMC. Previous *operando* studies of $Li_2MnO_3$ reported no evidence of an exotic $Mn^{4+/7+}$ redox mechanism,[21] but such a mechanism may potentially be stabilized when composited with classical layered oxides. To investigate, we performed *operando* Mn K-edge measurements of LR-NMC to probe the Mn redox activity (Figure S1). While Mn K-edge measurements give orders of magnitude lower energy transfer rates than Mn L-edge XAS and O K-edge RIXS (Table S1), we took additional precautions by cycling LR-NMC off-line and exposing to X-rays only when collecting data at predetermined charge points. In addition, we also measured $KMnO_4$ and precycled NMC 442 and NMC 811 electrodes, where no $Mn^{4+/7+}$ redox is expected, to serve as reference Mn spectra.

As shown in Figure 3a, Mn K-edge XANES data of $KMnO_4$ were obtained with no evidence of photoreduction while also being consistent with reports by others.[44−46] XANES spectra from pristine electrodes of LR-NMC, NMC 442, and NMC 811 show an almost identical $Mn^{4+}$ environment, with the vertical line indicating the 1s → 4p transition. The enlarged pre-edge inset associated with weak 1s → 3d transitions shows only subtle differences in the Mn−O hybridization, likely because of differences in composition and Ni valence. Unlike the cathode materials, $KMnO_4$ has a characteristically large pre-edge peak due to its tetrahedral $Mn^{7+}$ environment. Other high-valent Mn materials, such as $Mn^{5+}$ or $Mn^{6+}$, also prefer tetrahedral coordination. FEFF9Mn K-edge XANES simulations of $KMnO_4$ reproduce features found in experimentally obtained measurements (Figure S2). Using similar FEFF9 parameters, a hypothetical delithiated $Li_2MnO_3$ structure proposed by Radin *et al.*,[20] $Li_{1/2}MnO_3$, was also simulated and predicts a large pre-edge peak with intensity and energy similar to that of $KMnO_4$.

When charging to similar cutoff potential (4.75/4.80 V), all cathode materials exhibit large structural changes in the main edge, including a shift of the 4p peak to higher energy (Figure 3b). A less obvious, but more important, change in the Mn K-edge is the growth of pre-edge P1($t_{2g}$) and P2($e_g$) intensities for each system (Figure S3a). Our assingments of P1 and P2

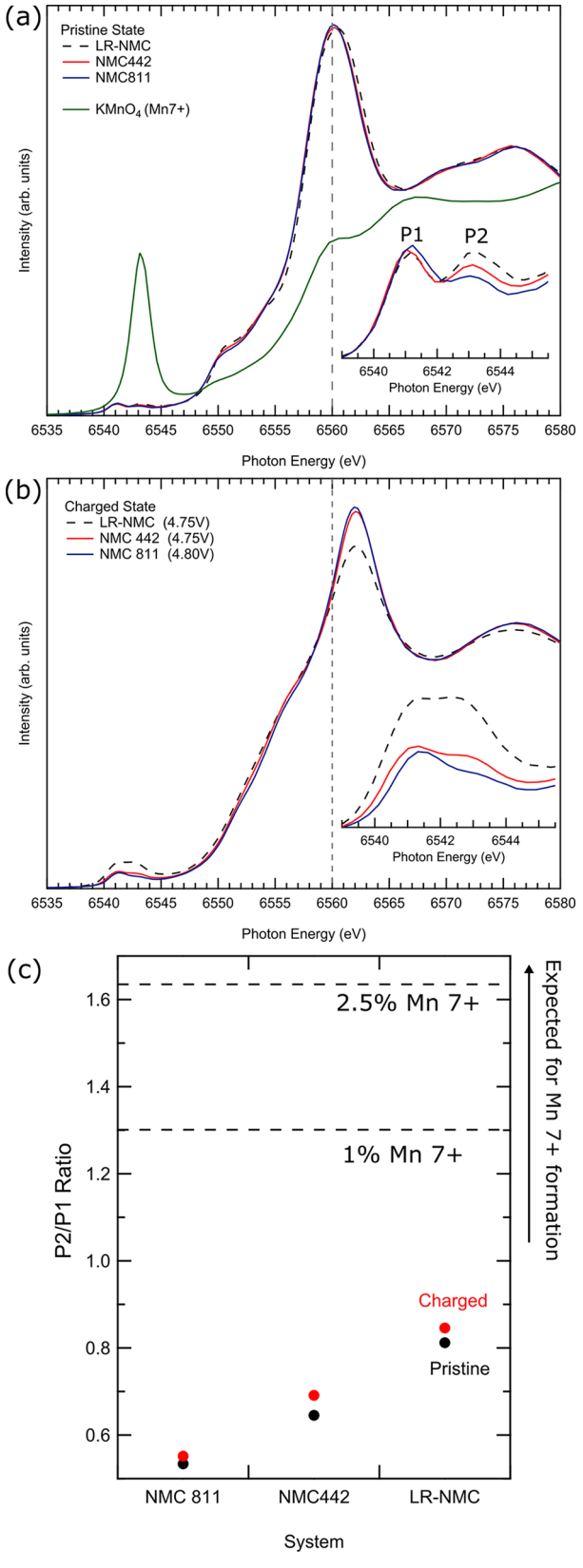


**Figure 3. Mn K-edge spectra of (a) pristine and (b) charged states of LR-NMC, NMC 442, and NMC 811. The spectrum of $KMnO_4$ is also plotted, which exhibits a large pre-edge feature. (c) Pre-edge P1($t_{2g}$) and P2($e_g$) peak intensity ratios are plotted. Horizontal lines indicated predicted peak ratio for 1% and 2.5% $Mn^{7+}$. Information on peak ratio predictions can be found in the Supporting Information.**

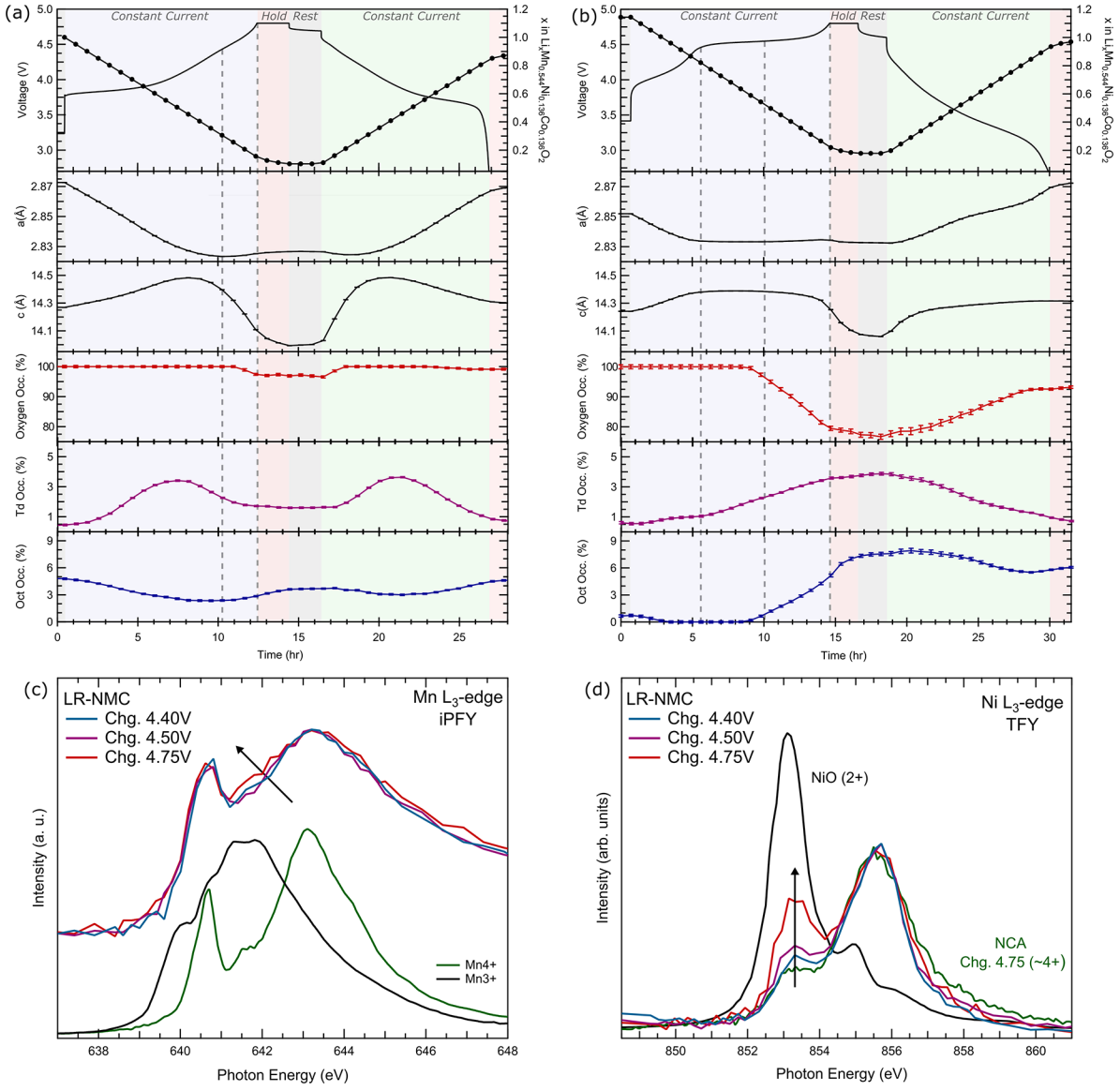


**Figure 4. First cycle *operando* XRD data including galvanostatic charge−discharge (4.75−2.7 V) curves, *a* and *c* lattice parameters, oxygen occupancy, and TM occupancy in Li layer of (a) LR-NMC and (b) NMC 442. (c) Mn L3-edge iPFY and (d) Ni L3-edge TFY of LR-NMC electrodes with Mn and Ni reference spectra.**

pre-edge peaks are 6541.15 and 6543.1 eV, respectively. The tetrahedral coordination of an emerging high-valent Mn (>4+) species would result in not only significant pre-edge growth but also a shift toward higher energy. To pinpoint changes in the pre-edge, the ratios of P1 and P2 peaks were taken and compared between pristine and charged states (Figure 3c). For classical layered oxides, the P2/P1 ratio shows very little deviation. For LR-NMC, there is negligible change in the overall P2/P1 ratio compared to what would be required for even 1% of $Mn^{7+}$ described by our theoretical model (Figure S3b). In addition, we note the similarity of main edge changes for LR-NMC to that of NMC 442/811, and the lack of significant pre-edge growth, as evidence of a limited high-valent Mn environments. This is consistent with all previous *operando*/*ex situ* XAS work done on Li-rich systems.[13,30,40,47,48]

Operando XRD measurements of NMC 442 and LR-NMC were performed to help quantify tetrahedral TM occupancy to complement our Mn K-edge XANES. First cycle NMC442 (Figure 4a) and LR-NMC (Figure 4b) display stark differences between lattice changes and electrochemical profiles. In the initial charge of NMC442, transition metal oxidation results in the shrinkage of transition metal−oxygen layer (*a* lattice) until reaching the high voltages. The lack of *a*-lattice changes, indicated by the two vertical lines, describe the end of Ni/Co oxidation in this system, consistent with our XANES studies. These *a*-lattice changes are accompanied by *c*-lattice growth and collapse. Our lattice parameter refinements are consistent with observations reported in the literature.[34,49] Both *a*- and *c*-lattice parameters show high degree of reversibility on discharge for NMC 442. For LR-NMC (Figure 4b), the *a*- and *c*-lattice trends are similar to a classical layered system until reaching the high-voltage plateau. During the high-voltage region, marked by three vertical lines, there are scarcely any further changes to *a*- and *c*-lattice parameters. We note that the corresponding Ni and Co K-edge XANES (Figures S4 and S5) also exhibit no evidence of further transition metal oxidation in this high-voltage regime. We note similar metal K-edge XANES spectral evolution in the high-voltage regimes of

NMC 442 that coincides with the onset of signatures of oxidized oxygen in RIXS in other classical layered oxides,[33] including NMC 333,[36] regardless of TM intermixing.

In addition to lattice parameters, concordant occupancy refinements were done for both octahedral and tetrahedral sites in the Li layer. Additional information regarding the fits is provided in the Supporting Information (Tables S2 and Figures S6−S15). NMC 442 prior to electrochemical cycling has some partially occupied octahedral sites by transition metals in the Li layer. We attribute this octahedral occupancy to TM/Li intermixing related to synthesis. More interestingly, during charging, NMC 442 displays a small decrease in cation intermixing and an increase in tetrahedral occupancy. For NMC 442, the highest occupancy of tetrahedral sites occurs at 0.5 delithiation, which then decreases when delithiating further. On the subsequent discharge, nearly symmetric changes are observed for tetrahedral and octahedral site occupancy in the Li layer. While tetrahedral coordination is also a requirement for a high-valent Mn(>4+) environment, no $Mn^{4+/7+}$ redox behavior in NMC 442 is expected. This leads us to interpret the transition metal migration within the Li layer in NMC 442 as being unrelated to a redox process. For NMC 442, our data suggest that (1) this processes has a high degree of reversibility and (2) tetrahedral migration and cation mixing is intrinsically linked based on the interplay of occupancy percentages. While XRD is less sensitive to oxygen occupancy, our refinements show very little change with the only change occurring at higher potentials where NMCs are increasingly thermodynamically prone to release oxygen.[50]

Returning to LR-NMC, there is also marginal transition metal occupancy in the Li layer of the initial starting materials, and it remains so during the classical transition metal redox region. During the high-voltage plateau region there is an increase in tetrahedral migration until the end of charge. Upon discharge, the tetrahedral occupancy decreases, suggesting this migratory process to be highly reversible. Reversible tetrahedral migration may suggest $Mn^{4+/7+}$ redox, but the small refined quantities are underwhelming for $Mn^{4+/7+}$ redox to be the dominant charge compensation mechanism. At approximately halfway across the high-voltage plateau there begins a significant increase in cation mixing while at the same time there is a significant decrease in oxygen occupancy. The increase in tetrahedral occupancy followed by increased cation mixing in tandem with oxygen fraction loss in the first charge suggests we are observing transition metal migration via the most thermodynamically favorable migration path of $TM_{oct} \rightarrow TM_{td} \rightarrow TM_{oct}$.[51] Even though the oxygen occupancy is partially recovered on discharge, there exists insignificant changes to cation mixing during discharge and on subsequent cycling (Figure S15). In addition, our refinements show the behavior of oxygen fraction is more intrinsically coupled to tetrahedral occupancy rather than octahedral occupancy after the first charge. This coupled tetrahedral and oxygen occupancy is also apparent upon subsequent cycles (Figure S15). In contrast to LR-NMC, NMC 442 shows a local minimum in tetrahedral occupancy at high charge states. Given that classical layered systems can also display oxidized oxygen RIXS signatures in the absence of transition metal migration,[33−36] we conclude that transition metal migration is not necessarily required to stabilize oxidized oxygen but may have an influence over oxygen redox behavior.

To comment on the refined oxygen (site) occupancy, we note that the sudden decrease in oxygen occupancy reported here does not trend with the gradual evolution of oxidized oxygen fraction first reported by Gent *et al.*[8] during the first charge of LR-NMC. This may be due to the sluggish kinetics of oxygen redox influencing *operando* measurements versus those of rested *ex situ* samples. Although XRD measurements cannot accurately describe the local environment of the oxygen atoms that have been displaced, local probes sensitive to short-range order such as neutron pair distribution function suggest the presence of a distorted oxygen sublattice.[40] In addition, the maximum oxygen occupancy loss (~20%) in this material far exceeds early estimates of oxygen loss from the lattice through DEMS studies of similar materials (~0.17$e^-$ per formula unit)[13] and therefore cannot fully account for the drop in oxygen fraction. Instead, we argue that the migration of transition metals into the Li layer causes a local displacement of oxygen atoms contributing to the observed loss of oxygen occupancy. This results in an inverse correlation between oxygen occupancy and TM occupancy in the Li layer. In terms of refinement, the decrease in oxygen occupancy can also be conveyed as an increase in the O site atomic displacement parameter (Figure S16). The incomplete recovery of oxygen occupancy on discharge can be rationalized by considering partial oxygen loss from the lattice and irreversible transition metal migration which occurred during charge.

After eliminating high-valent Mn as the source of tetrahedral migration observed in the LR-NMC XRD measurements, we now consider the possibility of Ni, Co, and/or lower-valence Mn migration that can correlate with the lower oxygen occupancy. In layered systems, $Mn^{3+}$ has the propensity to charge disproportionately into $Mn^{4+}$ and $Mn^{2+}$ containing spinel-like systems, where $Mn^{4+}$ favors octahedral occupancy and $Mn^{2+}$ favors tetrahedral occupancy on the surface.[52,53] At the same time, Mn migration from octahedral to tetrahedral sites is a key step in phase transformations of charged $Li_2MnO_3$ and $LiMn_2O_4$ into spinel-like structures.[54] Alternatively, $Ni^{3+/4+}$ and $Co^{3+}$ are not thermodynamically favorable in tetrahedral sites, but $Co^{2+}$ has been observed in tetrahedral sites by way of layered-to-spinel decomposition,[55] and $Ni^{2+}$ has been experimentally and thermodynamically shown to exist in tetrahedral sites.[56,57] On the basis of a purely thermodynamic/crystal field theory argument, $Co^{4+}$ can be either in the tetrahedral or octahedral site. In LR-NMC, our XRD refinements cannot accurately describe oxidation states, and for this reason we couple XRD with element-sensitive techniques describing the valence of migrating cations. Figure 4c shows bulk Mn L-edge (iPFY) absorption spectra of charged LR-NMC, where there is only some of $Mn^{4+}$ reducing to $Mn^{2+/3+}$. Although we report limited bulk Mn reduction, reduced Mn species have been reported on the surface of highly charged LR-NMC, NMC 442, and $Li_2MnO_3$ materials, likely brought on by oxygen loss and/or side reactions with electrolyte.[17] This leads us to believe that any possible tetrahedral $Mn^{2+}$, the result of charge disproportionation of $Mn^{3+}$, is likely to exist only at the surface. On the other hand, Ni L-edge spectra of LR-NMC show a more pronounced reduced $Ni^{2+}$ environment when highly charged (Figure 4d). While reduced surface Ni has also been reported for LR-NMC and NMC 442,[17] our more bulk sensitive Ni L-edge TFY measurements suggested this to be a more spacially extended $Ni^{2+}$ environment than that observed for classical layered oxides (*e.g.*, NCA) and constitutes ~20% of the overall bulk-sensitive Ni L-edge line shape. Given that reduced Ni at high potentials is also consistent with the correlated tetrahedral

occupancy and oxygen fraction, we consider low-valence Ni to be a partial contributor for tetrahedral occupancy. No signs of $Co^{2+}$ was observed in charged states of LR-NMC (Figure S17). While thermodynamically having no preference for tetrahedral sites, a low concentration of $Ni^{2+}$, $Co^{3+}/Co^{4+}$, and/or $Mn^{2+}/Mn^{3+}$ can become kinetically trapped because of the unavailability of an energetically favorable octahedral sites. The avalability of these sites can largely depend on Li content and degree of cation mixing. Kinetically trapped tetrahedral occupancy is also consistent with recent transmission electron microscopy (TEM) studies where there is densification and transition metal reduction near the surface and/or extended surface of particles.[17,58]

Recent work by Bruce *et al.* reported the formation of detached molecular oxygen trapped in a Li-rich compound without Mn oxidation as an intermediary step.[59] The formation of molecular oxygen is in good agreement with the loss of oxygen occupancy in LR-NMC. However, using the same refinement parameters used in LR-NMC, XRD measurements of classical layered oxides, such as NMC 442, show little change in the oxygen fraction. Classical layered oxides, in general, show little to no oxygen vacancies[60,61] while at the same time showing similar oxidized oxygen environments.[19,33−36] In addition, the RIXS spectra for electrochemically oxidized oxygen in LR-NMC is distinctly different from what is expected for molecular oxygen trapped in a cage (*e.g.*, irradiated $KMnO_4$). This suggests any molecular oxygen environment in LR-NMC must have a more complex framework within the cathode lattice than simply gas-phase molecular oxygen. These stark structural differences between Li-rich and classical layered samples in addition to the contrasting features in RIXS spectra is enough to warrant further study on the oxidized oxygen environment.

To conclude, this work quantifies the $Mn^{4+/7+}$ redox mechanism in LR-NMC and determines it to be insufficient to account for the excess of formal transition metal redox capacity observed. Oxygen K-edge RIXS measurements reveal $KMnO_4$ shares similar (but not all) RIXS signatures to that of LR-NMC, which questions the assignments of gas-phase molecular oxygen in LR-NMC. Moreover, X-ray exposure tests of $KMnO_4$ conclude the molecular oxygen feature to be beam-induced, which is not the case for LR-NMC. *Operando* XANES measurements show negligible evidence of $Mn^{4+/7+}$ redox occurring in LR-NMC during cycling, while our *operando* XRD measurements provide upper limits to the extent of tetrahedral/octahedral migration into the Li layer in both NMC 442 and LR-NMC. Transition metals stabilized in tetrahedral sites stabilized within the Li layer appear to be more consistent with lower-valence environments rather than a high-valent Mn species. Transition metal migration still remains an important issue for LR-NMC systems but is not necessarily promoting trapped gas-phase molecular oxygen formation induced by the degradation of $Mn^{4+/7+}$ redox. Taken together this suggests transition metal migration is not necessarily promoting oxygen redox, but suitable structural motifs may influence the stability of an oxidized oxygen environment.

## ■ ASSOCIATED CONTENT

### Supporting Information

The Supporting Information is available free of charge at https://pubs.acs.org/doi/10.1021/acsenergylett.0c02418.

Experimental details, including X-ray diffraction refinement parameters used; additional data, including max skin dose calculations, XANES/EXAFS of Mn, Co, Ni K-edges, FEFF9 simulations, Mn pre-edge analysis, Co $L_3$-edge, and PCA results (PDF)

## ■ AUTHOR INFORMATION


### Corresponding Author

**Louis F. J. Piper** − *Department of Physics, Binghamton University, Binghamton, New York 13905, United States; WMG, University of Warwick, Coventry CV4 7AL, United Kingdom;* orcid.org/0000-0002-3421-3210; Email: louis.piper@warwick.ac.uk

### Authors

**Mateusz Jan Zuba** − *NorthEast Center for Chemical Energy Storage at Binghamton University, Binghamton, New York 13902, United States;* orcid.org/0000-0002-3209-7922

**Antonin Grenier** − *Department of Chemistry, Stony Brook University, Stony Brook, New York 11794, United States*

**Zachary Lebens-Higgins** − *Department of Physics, Binghamton University, Binghamton, New York 13905, United States*

**Galo J. Paez Fajardo** − *Department of Physics, Binghamton University, Binghamton, New York 13905, United States;* orcid.org/0000-0003-0639-2896

**Yixuan Li** − *Department of Nano Engineering, University of California San Diego (UCSD), La Jolla, California 92093, United States*

**Yang Ha** − *Advanced Light Source, Lawrence Berkeley National Laboratory, Berkeley, California 94720, United States*

**Hui Zhou** − *NorthEast Center for Chemical Energy Storage at Binghamton University, Binghamton, New York 13902, United States*

**M. Stanley Whittingham** − *NorthEast Center for Chemical Energy Storage at Binghamton University, Binghamton, New York 13902, United States*

**Wanli Yang** − *Advanced Light Source, Lawrence Berkeley National Laboratory, Berkeley, California 94720, United States;* orcid.org/0000-0003-0666-8063

**Ying Shirley Meng** − *Department of Nano Engineering, University of California San Diego (UCSD), La Jolla, California 92093, United States*

**Karena W. Chapman** − *Department of Chemistry, Stony Brook University, Stony Brook, New York 11794, United States;* orcid.org/0000-0002-8725-5633

Complete contact information is available at: https://pubs.acs.org/10.1021/acsenergylett.0c02418


### Notes

The authors declare no competing financial interest.

## ■ ACKNOWLEDGMENTS


We thank A. Van der Ven and Daniil Kitchaev for insightful discussions. We acknowledge Argonne National Laboratory's Cell Analysis, Modeling, and Prototyping (CAMP) facility for providing the NMC442 powder. This work was supported as part of the NorthEast Center for Chemical Energy Storage (NECCES), an Energy Frontier Research Center funded by the U.S. Department of Energy, Office of Science, Office of Basic Energy Sciences, under Award No. DE-SC0012583.

L.F.J.P. also thanks the Scialog program from the Research Corporation for Science Advancement. The work at the ALS was supported by the Office of Basic Energy Sciences, of the U.S. Department of Energy, under Contract No. DE-AC02-05CH11231. This research used resources (Beamline 6BMM) of the National Synchrotron Light Source II (NSLS-II), a U.S. Department of Energy (DOE) Office of Science User Facility operated for the DOE Office of Science by Brookhaven National Laboratory under Contract No. DE- SC0012704. The authors gratefully acknowledge Dr. Bruce Ravel for his assistance during XAS experiments at beamline 6BMM of NSLS-II.

## REFERENCES

(1) Whittingham, M. S. Lithium batteries and cathode materials. *Chem. Rev.* **2004**, *104*, 4271−4301.

(2) Qiu, B.; Zhang, M.; Xia, Y.; Liu, Z.; Meng, Y. S. Understanding and Controlling Anionic Electrochemical Activity in High-Capacity Oxides for Next Generation Li-Ion Batteries. *Chem. Mater.* **2017**, *29*, 908−915.

(3) Rozier, P.; Tarascon, J. M. Review—Li-Rich Layered Oxide Cathodes for Next-Generation Li-Ion Batteries: Chances and Challenges. *J. Electrochem. Soc.* **2015**, *162*, A2490−A2499.

(4) Assat, G.; Foix, D.; Delacourt, C.; Iadecola, A.; Dedryvère, R.; Tarascon, J.-M. Fundamental interplay between anionic/cationic redox governing the kinetics and thermodynamics of lithium-rich cathodes. *Nat. Commun.* **2017**, 2219.

(5) Mohanty, D.; Li, J.; Nagpure, S. C.; Wood, D. L.; Daniel, C. Understanding the structure and structural degradation mechanisms in high-voltage, lithium-manganese-rich lithium-ion battery cathode oxides: A review of materials diagnostics. *MRS Energy & Sustainability* **2015**, *2*, E15.

(6) Li, Y.; Bettge, M.; Polzin, B.; Zhu, Y.; Balasubramanian, M.; Abraham, D. Understanding Long-Term Cycling Performance of Li1.2Ni0.15Mn0.55Co0.1O2-Graphite Lithium-Ion Cells. *J. Electrochem. Soc.* **2013**, *160*, A3006−A3019.

(7) Dogan, F.; Long, B. R.; Croy, J. R.; Gallagher, K. G.; Iddir, H.; Russell, J. T.; Balasubramanian, M.; Key, B. Re-entrant Lithium Local Environments and Defect Driven Electrochemistry of Li- and Mn-Rich Li-Ion Battery Cathodes. *J. Am. Chem. Soc.* **2015**, *137*, 2328−2335. PMID: 25634302.

(8) Gent, W. E.; Lim, K.; Liang, Y.; Li, Q.; Barnes, T.; Ahn, S.-j.; Stone, K. H.; McIntire, M.; Hong, J.; Song, J. H.; Li, Y.; Mehta, A.; Ermon, S.; Tyliszczak, T.; Kilcoyne, D.; Vine, D.; Park, J.-h.; Doo, S.-k.; Toney, M. F.; Yang, W.; Prendergast, D.; Chueh, W. C. Coupling between oxygen redox and cation migration explains unusual electrochemistry in lithium-rich layered oxides. *Nat. Commun.* **2017**, *8*, 2091.

(9) Qiu, B.; Zhang, M.; Lee, S.-Y.; Liu, H.; Wynn, T. A.; Wu, L.; Zhu, Y.; Wen, W.; Brown, C. M.; Zhou, D.; Liu, Z.; Meng, Y. S. Metastability and Reversibility of Anionic Redox-Based Cathode for High-Energy Rechargeable Batteries. *Cell Reports Physical Science* **2020**, *1*, 100028.

(10) Li, Y.; Zuba, M. J.; Bai, S.; Lebens-Higgins, Z. W.; Qiu, B.; Park, S.; Liu, Z.; Zhang, M.; Piper, L. F.J.; Meng, Y. S. Regeneration of degraded Li-rich layered oxide materials through heat treatment-induced transition metal reordering. *Energy Storage Materials* **2021**, *35*, 99−107.

(11) Li, X.; Qiao, Y.; Guo, S.; Xu, Z.; Zhu, H.; Zhang, X.; Yuan, Y.; He, P.; Ishida, M.; Zhou, H. Direct Visualization of the Reversible O 2 /O Redox Process in Li-Rich Cathode Materials. *Adv. Mater.* **2018**, *30*, 1705197.

(12) Qiao, Y.; Guo, S.; Zhu, K.; Liu, P.; Li, X.; Jiang, K.; Sun, C.-J.; Chen, M.; Zhou, H. Reversible anionic redox activity in Na3RuO4 cathodes: a prototype Na-rich layered oxide. *Energy Environ. Sci.* **2018**, *11*, 299−305.

(13) Luo, K.; Roberts, M. R.; Hao, R.; Guerrini, N.; Pickup, D. M.; Liu, Y.-s.; Edström, K.; Guo, J.; Chadwick, A. V.; Duda, L. C.; Bruce, P. G. Charge-compensation in 3d-transition-metal-oxide intercalation cathodes through the generation of localized electron holes on oxygen. *Nat. Chem.* **2016**, *8*, 684.

(14) Hong, J.; Gent, W. E.; Xiao, P.; Lim, K.; Seo, D. H.; Wu, J.; Csernica, P. M.; Takacs, C. J.; Nordlund, D.; Sun, C. J.; Stone, K. H.; Passarello, D.; Yang, W.; Prendergast, D.; Ceder, G.; Toney, M. F.; Chueh, W. C. Metal-oxygen decoordination stabilizes anion redox in Li-rich oxides. *Nat. Mater.* **2019**, *18*, 256−265.

(15) Yang, W.; Devereaux, T. P. Anionic and cationic redox and interfaces in batteries: Advances from soft X-ray absorption spectroscopy to resonant inelastic scattering. *J. Power Sources* **2018**, *389*, 188−197.

(16) Wu, J.; Li, Q.; Sallis, S.; Zhuo, Z.; Gent, W.; Chueh, W.; Yan, S.; Chuang, Y.-d.; Yang, W. Fingerprint Oxygen Redox Reactions in Batteries through High-Efficiency Mapping of Resonant Inelastic X-ray Scattering. *Condensed Matter* **2019**, *4*, 5.

(17) Lebens-Higgins, Z. W.; Chung, H.; Zuba, M. J.; Rana, J.; Li, Y.; Faenza, N. V.; Pereira, N.; McCloskey, B. D.; Rodolakis, F.; Yang, W.; Whittingham, M. S.; Amatucci, G. G.; Meng, Y. S.; Lee, T. L.; Piper, L. F. How Bulk Sensitive is Hard X-ray Photoelectron Spectroscopy: Accounting for the Cathode-Electrolyte Interface when Addressing Oxygen Redox. *J. Phys. Chem. Lett.* **2020**, *11*, 2106−2112.

(18) Wu, J.; Yang, Y.; Yang, W. Advances in soft X-ray RIXS for studying redox reaction states in batteries. *Dalton Transactions* **2020**, *49*, 13519−13527.

(19) House, R. A.; Maitra, U.; Pérez-Osorio, M. A.; Lozano, J. G.; Jin, L.; Somerville, J. W.; Duda, L. C.; Nag, A.; Walters, A.; Zhou, K.-J.; Roberts, M. R.; Bruce, P. G. Superstructure control of first-cycle voltage hysteresis in oxygen-redox cathodes. *Nature* **2020**, *577*, 502−508.

(20) Radin, M. D.; Vinckeviciute, J.; Seshadri, R.; van der Ven, A. Manganese oxidation as the origin of the anomalous capacity of Mn-containing Li-excess cathode materials. *Nature Energy* **2019**, *4*, 639−646.

(21) Rana, J.; Papp, J. K.; Lebens-Higgins, Z.; Zuba, M.; Kaufman, L. A.; Goel, A.; Schmuch, R.; Winter, M.; Whittingham, M. S.; Yang, W.; McCloskey, B. D.; Piper, L. F. J. Quantifying the Capacity Contributions during Activation of $Li_2MnO_3$. *ACS Energy Letters* **2020**, *5*, 634−641.

(22) Guerrini, N.; Jin, L.; Lozano, J. G.; Luo, K.; Sobkowiak, A.; Tsuruta, K.; Massel, F.; Duda, L.-C.; Roberts, M. R.; Bruce, P. G. Charging Mechanism of Li 2 MnO 3. *Chem. Mater.* **2020**, *32*, 3733−3740.

(23) Massel, F.; Hikima, K.; Rensmo, H.; Suzuki, K.; Hirayama, M.; Xu, C.; Younesi, R.; Liu, Y. S.; Guo, J.; Kanno, R.; Hahlin, M.; Duda, L. C. Excess Lithium in Transition Metal Layers of Epitaxially Grown Thin Film Cathodes of Li2MnO3 Leads to Rapid Loss of Covalency during First Battery Cycle. *J. Phys. Chem. C* **2019**, *123*, 28519−28526.

(24) Xu, J.; Sun, M.; Qiao, R.; Renfrew, S. E.; Ma, L.; Wu, T.; Hwang, S.; Nordlund, D.; Su, D.; Amine, K.; Lu, J.; McCloskey, B. D.; Yang, W.; Tong, W. Elucidating anionic oxygen activity in lithium-rich layered oxides. *Nat. Commun.* **2018**, *9*, 947.

(25) Renfrew, S. E.; McCloskey, B. D. Residual Lithium Carbonate Predominantly Accounts for First Cycle CO2 and CO Outgassing of Li-Stoichiometric and Li-Rich Layered Transition-Metal Oxides. *J. Am. Chem. Soc.* **2017**, *139*, 17853−17860.

(26) Chen, D.; Wu, J.; Papp, J. K.; McCloskey, B. D.; Yang, W.; Chen, G. Role of Redox-Inactive Transition-Metals in the Behavior of Cation-Disordered Rocksalt Cathodes. *Small* **2020**, *16*, 2000656.

(27) Gent, W. E.; Abate, I. I.; Yang, W.; Nazar, L. F.; Chueh, W. C. Design Rules for High-Valent Redox in Intercalation Electrodes. *Joule* **2020**, 1369.

(28) Lebens-Higgins, Z. W.; Vinckeviciute, J.; Wu, J.; Faenza, N. V.; Li, Y.; Sallis, S.; Pereira, N.; Meng, Y. S.; Amatucci, G. G.; Der Ven, A. V.; Yang, W.; Piper, L. F. J. Distinction between Intrinsic and X-ray-Induced Oxidized Oxygen States in Li-Rich 3d Layered Oxides and LiAlO2. *J. Phys. Chem. C* **2019**, *123*, 13201−13207.

(29) Qiu, B.; Zhang, M.; Wu, L.; Wang, J.; Xia, Y.; Qian, D.; Liu, H.; Hy, S.; Chen, Y.; An, K.; Zhu, Y.; Liu, Z.; Meng, Y. S. Gas-solid

interfacial modification of oxygen activity in layered oxide cathodes for lithium-ion batteries. *Nat. Commun.* **2016**, *7*, 12108.
(30) Koga, H.; Croguennec, L.; Ménétrier, M.; Mannessiez, P.; Weill, F.; Delmas, C.; Belin, S. Operando X-ray absorption study of the redox processes involved upon cycling of the li-rich layered oxide Li 1.20 Mn 0.54 Co 0.13 Ni 0.13 O 2 in li ion batteries. *J. Phys. Chem. C* **2014**, *118*, 5700−5709.
(31) Chen, H.; Islam, M. S. Lithium extraction mechanism in Li-rich Li2MnO3 involving oxygen hole formation and dimerization. *Chem. Mater.* **2016**, *28*, 6656−6663.
(32) Sudayama, T.; Uehara, K.; Mukai, T.; Asakura, D.; Shi, X.-M.; Tsuchimoto, A.; Mortemard de Boisse, B.; Shimada, T.; Watanabe, E.; Harada, Y.; Nakayama, M.; Okubo, M.; Yamada, A. Multiorbital bond formation for stable oxygen-redox reaction in battery electrodes. *Energy Environ. Sci.* **2020**, *13*, 1492−1500.
(33) Lebens-Higgins, Z. W.; Faenza, N. V.; Radin, M. D.; Liu, H.; Sallis, S.; Rana, J.; Vinckeviciute, J.; Reeves, P. J.; Zuba, M. J.; Badway, F.; Pereira, N.; Chapman, K. W.; Lee, T. L.; Wu, T.; Grey, C. P.; Melot, B. C.; Van Der Ven, A.; Amatucci, G. G.; Yang, W.; Piper, L. F. Revisiting the charge compensation mechanisms in LiNi0.8Co0.2-: YAlyO2 systems. *Mater. Horiz.* **2019**, *6*, 2112−2123.
(34) Li, N.; Sallis, S.; Papp, J. K.; Wei, J.; McCloskey, B. D.; Yang, W.; Tong, W. Unraveling the Cationic and Anionic Redox Reactions in a Conventional Layered Oxide Cathode. *ACS Energy Letters* **2019**, *4*, 2836−2842.
(35) Zhang, J. N.; Li, Q.; Ouyang, C.; Yu, X.; Ge, M.; Huang, X.; Hu, E.; Ma, C.; Li, S.; Xiao, R.; Yang, W.; Chu, Y.; Liu, Y.; Yu, H.; Yang, X. Q.; Huang, X.; Chen, L.; Li, H. Trace doping of multiple elements enables stable battery cycling of LiCoO2 at 4.6 V. *Nature Energy* **2019**, *4*, 594−603.
(36) Lee, G. H.; Wu, J.; Kim, D.; Cho, K.; Cho, M.; Yang, W.; Kang, Y. M. Reversible Anionic Redox Activities in Conventional LiNi1/3Co1/3Mn1/3O2 Cathodes. *Angew. Chem., Int. Ed.* **2020**, *59*, 8681−8688.
(37) Zhuo, Z.; Liu, Y. S.; Guo, J.; Chuang, Y. D.; Pan, F.; Yang, W. Full Energy Range Resonant Inelastic X-ray Scattering of O2 and CO2: Direct Comparison with Oxygen Redox State in Batteries. *J. Phys. Chem. Lett.* **2020**, *11*, 2618−2623.
(38) Glans, P.; Gunnelin, K.; Skytt, P.; Guo, J.-H.; Wassdahl, N.; Nordgren, J.; Ågren, H.; Gel'mukhanov, F. K.; Warwick, T.; Rotenberg, E. Resonant X-Ray Emission Spectroscopy of Molecular Oxygen. *Phys. Rev. Lett.* **1996**, *76*, 2448−2451.
(39) Zhuo, Z.; Pemmaraju, C. D.; Vinson, J.; Jia, C.; Moritz, B.; Lee, I.; Sallies, S.; Li, Q.; Wu, J.; Dai, K.; Chuang, Y. D.; Hussain, Z.; Pan, F.; Devereaux, T. P.; Yang, W. Spectroscopic Signature of Oxidized Oxygen States in Peroxides. *J. Phys. Chem. Lett.* **2018**, *9*, 6378−6384.
(40) Zhao, E.; Zhang, M.; Wang, X.; Hu, E.; Liu, J.; Yu, X.; Olguin, M.; Wynn, T. A.; Meng, Y. S.; Page, K.; Wang, F.; Li, H.; Yang, X.-Q.; Huang, X.; Chen, L. Local structure adaptability through multi cations for oxygen redox accommodation in Li-Rich layered oxides. *Energy Storage Materials* **2020**, *24*, 384−393.
(41) van Schooneveld, M.; DeBeer, S. A close look at dose: Toward L-edge XAS spectral uniformity, dose quantification and prediction of metal ion photoreduction. *J. Electron Spectrosc. Relat. Phenom.* **2015**, *198*, 31−56.
(42) Århammar, C.; Pietzsch, A.; Bock, N.; Holmström, E.; Araujo, C. M.; Gråsjö, J.; Zhao, S.; Green, S.; Peery, T.; Hennies, F.; Amerioun, S.; Föhlisch, A.; Schlappa, J.; Schmitt, T.; Strocov, V. N.; Niklasson, G. A.; Wallace, D. C.; Rubensson, J. E.; Johansson, B.; Ahuja, R. Unveiling the complex electronic structure of amorphous metal oxides. *Proc. Natl. Acad. Sci. U. S. A.* **2011**, *108*, 6355−6360.
(43) Herbstein, G. R.; Weissman, A. Lis 1.1.0. *Inorg. Phys. Theor.* **1971**, *566*, 5−10.
(44) Bianconi, A.; Garcia, J.; Benfatto, M.; Marcelli, A.; Natoli, C. R.; Ruiz-Lopez, M. F. Multielectron excitations in the K-edge x-ray-absorption near-edge spectra of V, Cr, and Mn 3d0 compounds with tetrahedral coordination. *Phys. Rev. B: Condens. Matter Mater. Phys.* **1991**, *43*, 6885−6892.
(45) Muller-Bouvet, D.; Emery, N.; Tassali, N.; Panabière, E.; Bach, S.; Crosnier, O.; Brousse, T.; Cénac-Morthe, C.; Michalowicz, A.; Pereira-Ramos, J. P. Unravelling redox processes of Li7MnN4 upon electrochemical Li extraction-insertion using operando XAS. *Phys. Chem. Chem. Phys.* **2017**, *19*, 27204−27211.
(46) Rana, J.; Stan, M.; Kloepsch, R.; Li, J.; Schumacher, G.; Welter, E.; Zizak, I.; Banhart, J.; Winter, M. Structural Changes in Li2MnO3Cathode Material for Li-Ion Batteries. *Adv. Energy Mater.* **2014**, *4*, 1300998.
(47) Ito, A.; Sato, Y.; Sanada, T.; Hatano, M.; Horie, H.; Ohsawa, Y. In situ X-ray absorption spectroscopic study of Li-rich layered cathode material Li[Ni0.17Li0.2Co0.07Mn 0.56]O2. *J. Power Sources* **2011**, *196*, 6828−6834.
(48) Wang, L.; Dai, A.; Xu, W.; Lee, S.; Cha, W.; Harder, R.; Liu, T.; Ren, Y.; Yin, G.; Zuo, P.; Wang, J.; Lu, J.; Wang, J. Structural distortion induced by manganese activation in a lithium-rich layered cathode. *J. Am. Chem. Soc.* **2020**, *142*, 14966−14973.
(49) Kondrakov, A. O.; Geßwein, H.; Galdina, K.; de Biasi, L.; Meded, V.; Filatova, E. O.; Schumacher, G.; Wenzel, W.; Hartmann, P.; Brezesinski, T.; Janek, J. Charge-transfer-induced lattice collapse in Ni-rich NCM cathode materials during delithiation. *J. Phys. Chem. C* **2017**, *121*, 24381.
(50) Xiong, D. J.; Ellis, L. D.; Li, J.; Li, H.; Hynes, T.; Allen, J. P.; Xia, J.; Hall, D. S.; Hill, I. G.; Dahn, J. R. Measuring Oxygen Release from Delithiated LiNi x Mn y Co 1-x-y O 2 and Its Effects on the Performance of High Voltage Li-Ion Cells. *J. Electrochem. Soc.* **2017**, *164*, A3025−A3037.
(51) Reed, J.; Ceder, G. Role of electronic structure in the susceptibility of metastable transition-metal oxide structures to transformation. *Chem. Rev.* **2004**, *104*, 4513−4533.
(52) Reed, J.; Ceder, G.; van der Ven, A. Layered-to-spinel phase transition in LixMnO2. *Electrochem. Solid-State Lett.* **2001**, *4*, 78−81.
(53) Benedek, R.; Thackeray, M. M. Simulation of the surface structure of lithium manganese oxide spinel. *Phys. Rev. B: Condens. Matter Mater. Phys.* **2011**, *83*, 195439.
(54) Kan, Y.; Hu, Y.; Lin, C. K.; Ren, Y.; Sun, Y. K.; Amine, K.; Chen, Z. Migration of Mn cations in delithiated lithium manganese oxides. *Phys. Chem. Chem. Phys.* **2014**, *16*, 20697−20702.
(55) Bak, S. M.; Hu, E.; Zhou, Y.; Yu, X.; Senanayake, S. D.; Cho, S. J.; Kim, K. B.; Chung, K. Y.; Yang, X. Q.; Nam, K. W. Structural changes and thermal stability of charged LiNixMnyCozO2 cathode materials studied by combined in situ time-resolved XRD and mass spectroscopy. *ACS Appl. Mater. Interfaces* **2014**, *6*, 22594−22601.
(56) Ahmed, S.; Bianchini, M.; Pokle, A.; Munde, M. S.; Hartmann, P.; Brezesinski, T.; Beyer, A.; Janek, J.; Volz, K. Visualization of Light Elements using 4D STEM: The Layered-to-Rock Salt Phase Transition in LiNiO2 Cathode Material. *Adv. Energy Mater.* **2020**, *10*, 2001026.
(57) Schipper, F.; Dixit, M.; Kovacheva, D.; Talianker, M.; Haik, O.; Grinblat, J.; Erickson, E. M.; Ghanty, C.; Major, D. T.; Markovsky, B.; Aurbach, D. Stabilizing nickel-rich layered cathode materials by a high-charge cation doping strategy: Zirconium-doped LiNi0.6-Co0.2Mn0.2O2. *J. Mater. Chem. A* **2016**, *4*, 16073−16084.
(58) Yin, W.; Grimaud, A.; Rousse, G.; Abakumov, A. M.; Senyshyn, A.; Zhang, L.; Trabesinger, S.; Iadecola, A.; Foix, D.; Giaume, D.; Tarascon, J.-M. Structural evolution at the oxidative and reductive limits in the first electrochemical cycle of Li1.2Ni0.13Mn0.54-Co0.13O2. *Nat. Commun.* **2020**, *11*, 1252.
(59) House, R. A.; Rees, G. J.; Pérez-Osorio, M. A.; Marie, J.-J.; Boivin, E.; Robertson, A. W.; Nag, A.; Garcia-Fernandez, M.; Zhou, K.-J.; Bruce, P. G. First-cycle voltage hysteresis in Li-rich 3d cathodes associated with molecular O2 trapped in the bulk. *Nature Energy* **2020**, *5*, 777−785.
(60) Yin, S. C.; Rho, Y. H.; Swainson, I.; Nazar, L. F. X-ray/neutron diffraction and electrochemical studies of lithium De/Re-intercalation in Li1-xCo1/3Ni1/3Mn 1/3O2 (x = 0 1). *Chem. Mater.* **2006**, *18*, 1901−1910.
(61) Liu, H.; Liu, H.; Lapidus, S. H.; Meng, Y. S.; Chupas, P. J.; Chapman, K. W. Sensitivity and Limitations of Structures from X-ray

and Neutron-Based Diffraction Analyses of Transition Metal Oxide Lithium-Battery Electrodes. *J. Electrochem. Soc.* **2017**, *164*, A1802–A1811.